Journal Pre-proof

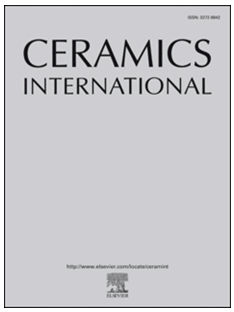

Accelerated crystallization of $CuAlO_2$ delafossite phase by controlling thermal regime during solution combustion synthesis

Elham Garmroudi Nezhad, Sahar Mollazadeh Beidokhti, Jalil Vahdati-Khaki

PII: S0272-8842(20)31325-0

DOI: https://doi.org/10.1016/j.ceramint.2020.05.040

Reference: CERI 25141

To appear in: *Ceramics International*

Received Date: 24 January 2020

Revised Date: 29 April 2020

Accepted Date: 3 May 2020

Please cite this article as: E.G. Nezhad, S.M. Beidokhti, J. Vahdati-Khaki, Accelerated crystallization of $CuAlO_2$ delafossite phase by controlling thermal regime during solution combustion synthesis, *Ceramics International* (2020), doi: https://doi.org/10.1016/j.ceramint.2020.05.040.

Accelerated crystallization of $CuAlO_2$ delafossite phase by controlling thermal regime during solution combustion synthesis

Elham Garmroudi Nezhad, Sahar Mollazadeh Beidokhti, Jalil Vahdati-Khaki*

Department of Materials Science and Engineering, Engineering Faculty, Ferdowsi University of Mashhad, Mashhad, Iran

*Corresponding author: Jalil Vahdati-Khaki (vahdati@um.ac.ir).

Abstract

In the present study, for the first time, $CuAlO_2$ delafossite phase was successfully obtained through a one-step solution combustion synthesis (SCS) process. Moreover, in order to accelerate $CuAlO_2$ crystallization, two-step process, i.e. SCS followed by heat-treatment (different thermal regimes: continuous and discontinuous) without controlling the atmospheric oxygen, was applied. In the two-step process, heating time duration needed for the crystallization of $CuAlO_2$ was lowered to 30 minutes at 1100ºC by exerting SCS on the mixture of starting materials. It was found that different thermal regimes can highly affect the formation of $CuAlO_2$ phase. Furthermore, according to the SEM and TEM studies, it was revealed that the resultant powders have a flaky-shape morphology with lamellar structure.

Keywords:

$CuAlO_2$, Thermal regimes, In-situ XRD, Solution combustion synthesis, $CuAl_2O_4$

1- Introduction

In order to satisfy the world's fast-growing energy demand, developing inexpensive materials for energy conversion and storage is a vital need. Accordingly, significant efforts have been devoted in developing different n- and p-type oxide semiconductors. Since the P-type oxides with strong conductivity as well as transparency across the visible spectrum are scant, special attention is paid to their production [1]. A few p-type oxides have been interested, including $CuAlO_2$ [1], $SrCu_2O_2$ [2], LaCuOSe [3] and As-doped ZnO [4]. Among the mentioned oxides, cuprous aluminate delafossite ($CuAlO_2$) is a good candidate because of its p-type conductivity without intentional doping as well as the abundance of the constituent elements [5]. Delafossite $CuAlO_2$ belongs to a family of transparent conducting oxides (TCOs), possessing low electrical resistivity and high visual light transparency which shows promising properties in various applications such as liquid crystal displays, thermoelectric devices, light-emitting diodes and so on [6, 7].

Different techniques have been utilized to produce $CuAlO_2$ nanoparticles including sol-gel [8,9], mechanical alloying [10], hydrothermal [11], solid-state routes [12], sputtering [13], solution combustion synthesis (SCS) [14] and electro-spinning method [15]. Among them, SCS is a time- as well as energy-saving strategy, especially, in the preparation of complex oxides when compared with other techniques and can be highly used for scale-up applications [16–19]. Nano-crystalline oxides can be produced via the redox reaction between an oxidizer containing the metal precursor/precursors and an organic fuel at a moderately low initiation temperature of about 300–600ºC within a few minutes [16]. Producing powder particles with a high shape homogeneity of final products could be considered as another advantage of SCS route [20]. In addition, Li et al. reported that molecular level homogeneity can be obtained during production of metal oxide nanomaterials via SCS [16]. According to another study [21], nanostructured $ZnCo_2O_4$ was successfully produced through SCS from $Zn(NO_3)_2.6H_2O$, $Co(NO_3)_2.6H_2O$ and glycine. It was also reported that the final sintered sample has the most promising performance due to the excellent diffusion obtained by additional gas generation during the combustion process. $CuAlO_2$ delafossite phase was also produced by SCS followed by heat-treatment at 1000ºC for a long holding time of around 5 hours which is really time-consuming, and unfortunately,

annihilate the rapid nature of SCS[14]. However, to the best of our knowledge, $CuAlO_2$ single-phase has not yet been produced by using just SCS.

Delafossite $CuAlO_2$ is normally prepared by solid-state synthesis technique from CuO/Cu_2O and Al_2O_3 powder mixtures [12]. However, the presence of secondary phases as well as low relative densities have been highly reported for delafossite $CuAlO_2$, which was produced through solid-state synthesis, drastically affecting the properties of the resultant material [12,19]. Furthermore, high processing temperature as well as extremely long processing durations (from several hours up to several days) have been reported in the literatures [6,7]. As an instance, poly-crystalline $CuAlO_2$ was prepared through heating the stoichiometric powder mixture of Al_2O_3 and Cu_2O at 1100ºC for 4 days in Ar atmosphere [6]. In another study, Ahmed et al. [7] synthesized delafossite $CuAlO_2$ nanoparticles via sol-gel process. In the mentioned study, an aqueous solution of $Cu(NO_3)_2 2.5H_2O$ together with $Al(NO_3)_3.9H2O$ were mixed and then transferred to a crucible containing citric acid and ethylene glycol. After that, the solution was allowed to gel for a long time (3 days) at room temperature. In order to remove the organic chelating agents, a thermal treatment was done at a temperature of 350ºC for 6 hours in air, and finally, copper (II) oxide powder and an amorphous Al-based compound were produced. The powders were then fired at 775ºC for 12 h in the air leading to the formation of CuO and $CuAl_2O_4$. The resultant powder was also treated at 800ºC in ultrapure N_2 for 48 h, to get pure $CuAlO_2$ nanoparticles. The applied methods are so complex and time-consuming, and therefore, it is of interest to adopt a simple and rapid technique.

On the other hand, selecting an appropriate temperature and time as well as a proper atmosphere of the solid-state reaction are really important. Especially, in the powder mixture, the valence state of Cu ions should be controlled during heating and cooling regimes. Oxidation of Cu^+ to Cu^{2+} ions could occur during air-heating at relatively low temperatures ranging from 200 to 500ºC. Then, CuO compound starts to react with Al_2O_3, forming $CuAl_2O_4$ at temperatures below 1100ºC as follows:

$$Cu_2O + 1/2O_2 \rightarrow 2CuO \qquad (1)$$

$$CuO + Al_2O_3 \rightarrow CuAl_2O_4 \qquad (2)$$

It is reported that with further heating of the material, $CuAlO_2$ could be formed based on the following reaction:

$$CuO + CuAl_2O_4 \rightarrow 2CuAlO_2 + 1/2O_2 \quad (3)$$

Moreover, CuO decomposes moderately and will evaporate by heating above 1100ºC. However, the mentioned reason in addition to the presence of oxygen causes the above reaction shift backward, re-forming $CuAl_2O_4$. Other studies [20-22], showed that the reduction of CuO and $CuAl_2O_4$ can be occurred above 1020ºC, as follows:

$$2CuO \rightarrow Cu_2O + 1/2\ O_2 \qquad (4)$$

$$4CuAl_2O_4 \rightarrow 4CuAlO_2 + 2Al_2O_3 + O_2 \quad (5)$$

The other possible mechanism for the formation of $CuAlO_2$ can be shown as follows:

$$Cu_2O + Al_2O_3 \rightarrow 2CuAlO_2 \qquad (6)$$

Beside the above-mentioned mechanisms, it was also reported that $CuAlO_2$ could be directly achieved by reacting Cu_2O and Al_2O_3 at temperatures above 800ºC [24]. The formation of $CuAlO_2$ through the reaction of 6 agrees with the previous research by Jacob and Alcock on the formation and decomposition kinetics of $CuAlO_2$ [23]. It is worth noting that the reaction through which the delafossite $CuAlO_2$ can be formed is highly dependent on precursors. A summary of the above-mentioned reactions including reactants, intermediate phases as well as final products is provided in **Table 1**.

Table 1.

As mentioned before, crystallization of $CuAlO_2$ was a complex process requiring high temperatures as well as long durations. Accordingly, the applied techniques could not impart the benefit of rapid nature of SCS. Although SCS provides high temperatures, its rapid nature is a main challenge for producing $CuAlO_2$. For this reason, after applying SCS, heat-treatment is usually used in order to get the pure phase [16,17,23]. In this regard, in the present study, the possibility of the formation of pure delafossite phase through a one-step SCS process as well as SCS process followed by heat-treatment was evaluated. In order to examine the effect of temperature and oxygen partial pressure (OPP) on the resultant phase of the combustion-synthesized precursors, three different conditions were applied at the SCS stage as follows: preparing the precursors (i) on a hot-plate (300ºC, opened-system), (ii) on a hot-plate (300ºC, closed-system) and (iii) in a furnace (500ºC). In order to decrease the OPP, closed-system was used to evaluate its effect on the phase composition of the precursors. After preparing the precursors, different thermal regimes were applied at heat-treatment stage to evaluate their effects on the formation of delafossite phase. The phase purity and the

morphology of the resultant powders were studied by X-ray diffraction (XRD) technique, in-situ XRD as well as scanning electron microscopy (SEM) and transmission electron microscopy (TEM). Finally, $CuAlO_2$ single-phase was successfully produced via both applied approaches, namely one-step SCS and SCS followed by heat-treatment

2- Experimental procedure

In order to synthesize $CuAlO_2$ powder sample via solution combustion method, copper (II) nitrate hexahydrate (Sigma Aldrich; $Cu(NO_3)_2.3H_2O$, purity>99.9%) and aluminum nitrate nonahydrate (Merck; $Al(NO_3)_3.9H_2O$, purity>99.9%) as well as hexamine (Merck; $C_6H_{12}N_4$, purity>99.9%) were used as oxidizers and fuel, respectively. The following reactions were utilized to get one mole of $CuAlO_2$:

$$Cu(NO_3)_2.3H_2O+0.305C_6H_{12}N_4 \rightarrow 0.5Cu_2O+4.833H_2O+1.833CO_2+1.611N_2 \quad (7)$$

$$Al(NO_3)_3.9H_2O+0.416C_6H_{12}N_4 \rightarrow 0.5Al_2O_3+11.5H_2O+2.5CO_2+2.333N_2 \quad (8)$$

$$Al(NO_3)_3.9H_2O+Cu(NO_3)_2.3H_2O+0.7215C_6H_{12}N_4 \rightarrow CuAlO_2+16.33H_2O+4.329CO_2+3.944N_2 \quad (9)$$

It is worth mentioning that Eq. (9) is obtained by sum of Eq. (7) and Eq. (8). Calculated amounts of nitrates and fuel together with 4 cc deionized water were mixed through a magnetic stirrer for around 5 minutes. Two different approaches were adopted to synthesize the delafossite phase; one-step process (SCS) and SCS followed by heat-treatment (two-step). In the two-step method, solution combustion synthesis of $CuAlO_2$ was developed at three different conditions. First, the combustion synthesis process was conducted on a hotplate at 300ºC in air atmosphere (referred as H). In the second condition, the applied method was the same as before, but the used alumina crucible was closed by a lid immediately after observing the combustion flame and this condition was kept till the system got cold. The samples produced at this condition were referred to as CH. In the third condition, combustion was carried out in a furnace at 500ºC and the crucible was air-quenched just after the combustion (referred as F). After preparing the precursors, different thermal regimes were applied in order to investigate their effects on the possible formation of delafossite phase in the as-combustion synthesized samples. In this regard, continuous and discontinuous heating were adopted. As a continuous regime, the precursors were heat-

treated from ambient temperature to 1100°C in furnace with a heating rate of 5°C/min and were held for 1, 3 and 5 hours and finally air-quenched. It is worth noting that the used ceramic crucible was not covered by a lid in the furnace. From now on, H1, H3, H5 and CH1, CH3, CH5 as well as F1, F3 and F5 correspond to the before mentioned samples (precursors) heated for 1, 3 and 5 h, respectively. In order to better understand the compositional changes during continuous heat-treatment, CH samples (as representative) were heated and taken out from the furnace immediately after the target temperatures (400, 600, 700, 800, 900, 1000 and 1100ºC) being reached and were cooled in air. As another thermal regime (discontinuous), the samples (referred to as H0.5, CH0.5 and F0.5) were directly placed into the furnace at 1100ºC being kept for 30 minutes and air quenched immediately to investigate the possible formation of delafossite phase. Again, for better understanding chemical composition changes, discontinuous heating was applied for CH sample at different temperatures (400, 600, 700, 800, 900, 1000 and 1100ºC) for 30 minutes. On the other hand, in the one-step process, the magnetic-stirred solutions were directly placed in the preheated-furnace with temperatures of 1000, 1100, 1200 and 1250ºC and then were taken out from the furnace immediately after the SCS process was done and were cooled in air. Schematic illustration of all the applied processes is depicted in **Fig. 1**. The resultant phases were identified by X-ray diffraction (XRD) with CuKα radiation through Phillips X'Pert Pro X-ray diffractometer. In addition, in-situ XRD was also performed with a heating rate of 5ºC/min to study phase composition changes in CH sample from room temperatures up to 1100ºC at the target temperatures of 400, 600, 700, 800, 900, 1000 and 1100ºC. It should be mentioned that the time required to get XRD pattern at each temperature was around 30 minutes. It is worth noting that a strip heater chamber (Anton Paar HTK 16N) was used for *in-situ* powder X-ray diffraction at temperatures up to 1100ºC in air. Moreover, two thermocouples were utilized for accurate temperature measurement and control. Furthermore, the morphology of the produced samples was investigated with a SEM using field-emission gun (FESEM, MIRA3, TESCAN, CZ) and a transmission electron microscope (TEM, Philips, EM208S) at an accelerating voltage of 100 keV. In addition, differential thermal analysis (DTA, LINSEIS) as well as thermogravimetric analysis (TG, LINSEIS) were carried out on the samples in air condition with a heating rate of 5ºC/min in the temperature range of 25-1100ºC.

Fig. 1.

3- Results and discussion

3-1- Precursor characterization

3-1-1- Compositional and morphological characterization

In order to evaluate the resultant phases of the solution combustion synthesized samples, XRD analysis was used. The XRD patterns of the precursors prepared at different conditions (H, CH and F) are provided in **Fig. 2a**. As can be seen, the pattern of H sample mainly contains of Cu_2O (ICDD 01-078-2076, 2θ=36.441) as well as a few Cu (ICDD 01-085-1326, 2θ=43.317) peaks. The presence of Cu_2O is confirmed by the dominant peaks located at 36.44º, 42.329º and 61.408º corresponding to the (111), (200) and (220) planes of the oxide, respectively. Furthermore, according to CH sample, $CuAlO_2$ (ICDD 01-076-2398, 2θ=37.854), Cu_2O and Cu peaks can be observed in the corresponding pattern. It should be mentioned that the dominant peaks located at 43.317º, 50.449º and 74.126º corresponding to the (111), (200) and (220) planes of Cu element, respectively. However, the intensity of Cu and Cu_2O peaks are, respectively, higher and lower than that of H pattern. Furthermore, Al_2O_3 (ICDD 01-071-1124, 2θ=35.197) peaks can also be seen in CH and F patterns, which was produced from $Al(NO_3)_3.9H_2O$ through Eq. (8). It is worth mentioning that the dominant peaks in the XRD pattern of sample F belong to Cu_2O and Cu, as indexed before. Comparing XRD curves of **Fig. 2a**, it is revealed that the intensity of Cu characteristic peaks is higher in F and CH samples in comparison with H. It should be mentioned that during combustion process the decrease of oxygen partial pressure (OPP) is occurred [24,25]. Moreover, based on **Fig. 2b**, decreasing OPP as well as increasing temperature change the stability area, promoting the reduction of CuO to Cu_2O and Cu. Therefore, at a constant combustion temperature, since the OPP is lower in the closed-system comparing with the open one (H sample), the intensity of copper peaks is higher in CH sample. Furthermore, based on **Fig. 2c**, it should be said that the adiabatic temperatures theoretically increase from 1775ºC to 1801ºC and then to 1844ºC with increasing initial temperatures from 25ºC to 300ºC and to 500ºC, respectively. For this reason, higher adiabatic temperature of F sample at a constant OPP caused more amount of Cu to be formed in F sample in comparison with H. In addition, comparing closed-system (CH) with the open one (H), it can be deduced that being at

combustion temperature for longer time caused a slow cooling rate for the samples, and therefore, kinetically facilitate the formation of delafossite phase ($CuAlO_2$). Furthermore, in the F sample, some peaks are denoted as $CuAlO_2$ which could reveal the formation of delafossite phase. Higher processing temperature of F sample provides longer time for the powder being cooled, and therefore, may promote the formation of $CuAlO_2$.

Fig.2.

In order to better understand the microstructure of the powders synthesized by SCS process, SEM was used and the corresponding micrographs of H, CH and F precursors are presented in **Fig. 3a-h**. Featureless morphologies of the powders in **Fig. 3b**, **f** and **g** could be attributed to non-fully crystallized $Cu_xAl_yO_z$ phases (see EDS analysis results as an inset). However, after applying heat-treatment, the mentioned phases were fully crystallized possessing lamellar structures which will be discussed later. Nevertheless, an almost lamellar structure is observed in CH precursor (**Fig. 3d**) which may be attributed to the delafossite phase as was confirmed by the corresponding XRD pattern of **Fig. 2a**. It is worth mentioning that the dispersed nanoparticles in **Fig. 3c** could be Al_2O_3 phases. Based on the EDS result (inset of **Fig. 3c**), the intensity of Al element is higher for the area containing the mentioned nanoparticles. In addition, according to the literatures [26-28], the semi-spherical lumps presented in all three samples (marked by dashed-circles in **Fig. 3a**, **e** and **h**) correspond to Cu_2O phase. It is worth mentioning that the EDS analysis taken from the marked area in **Fig. 3e** shows higher amounts of copper. Moreover, some fine nanoparticles/plates in F sample can be observed on the Cu_2O lumps (marked by an arrow in **Fig. 3e**) being referred to CuO phases. It was also reported that CuO (ICDD 01-074-1021, 2θ=36.837) phase could be formed on the surface of Cu_2O, after absorbing oxygen from environment through superficial microcracks of Cu_2O [26-28]. Schematic illustration of Cu_2O oxidation is provided in **Fig. 3i**. Since F precursor experienced higher temperatures, the sample needed more time to be cooled, therefore, oxygen atoms could penetrate through the microcracks and formed CuO phase. The presence of CuO was confirmed earlier by XRD results of F sample in **Fig. 2a**.

Fig. 3.

3-1-2- Thermal stability

Figure 4a, **b** and **c** show the results of DTA and TG measurements conducted on H, F and CH powder samples, respectively. The first weight loss in TG results could be due to the

absorbed moisture removal. As can be seen in the DTA curves, there are exothermic peaks (1) located at 250ºC, accompanied with the weight loss which could be attributed to the released gases from the residual fuel. It should be also said that the following weight gains in TG results could be due to the oxidation of Cu and Cu_2O to CuO [31]. It has been reported that the oxidation of Cu^+ to Cu^{2+} ions could occur during heating in air at temperatures ranging from 200 to 500ºC, which is consistent with the present results. Moreover, there is also an endothermic peak at 620ºC (marked by 2 in **Fig. 4**) which may be attributed to residual nitrates decomposition. It was confirmed that the decomposition of pure $Cu(NO_3)_2.3H_2O$ is terminated at around 300ºC [31]. In addition, thermal decomposition of aluminum nitrate took place and extended to around 400ºC based on the literature [32]. However, the literature results were achieved for pure nitrates possessing thermodynamic activity equal 1. Since decreasing the activity increases the decomposition temperature, therefore, residual nitrate decomposition was occurred at around 600ºC, in the present study. Another observed exothermic peak (number 3) is located at around 950ºC, accompanied with a small weight loss, which may correspond to the oxidation of residual carbon doped in the powder mixture structure. In the powder mixture, the surrounded materials around the residual carbon may postpone the oxidation temperature to above 900ºC. The final endothermic peak (4) with a sharp weight reduction can be seen at 1020ºC corresponding to the formation of $CuAlO_2$ delafossite phase which is consistent with the results of other researches [22, 29]. As the transformation temperature of CuO to Cu_2O is 1020ºC [12], it may be deduced that the reduction of CuO as well as the formation of delafossite phase could take place simultaneously at around 1000ºC [16,19,22].

Fig. 4.

3-2- Two-step process: SCS followed by heat-treatment

3-2-1- Continuous heating

As mentioned in the experimental section, among the precursors, CH sample was selected as a representative for detailed investigations. The reason can be attributed to the distinct lamellar microstructure of CH precursor (**Fig. 3d**) as well as sharper $CuAlO_2$ peaks in the corresponding XRD pattern (**Fig. 2a**). In this regard, continuous heating was performed from room temperature up to 1100ºC with a heating rate of 5ºC/min, as shown in **Fig. 5a**. It is worth noting that the samples were taken out from the furnace immediately after the target

temperatures (400, 600, 700, 800, 900, 1000 and 1100ºC) being reached and were cooled in air. Furthermore, **Fig. 5b** shows the XRD results of CH sample after continuous heat-treatment. Furthermore, XRD pattern of the corresponding precursor is also provided in the figure as an indicator. As can be seen, the high intensity peaks of Cu phase are also observed at 400ºC together with CuO and Cu_2O phases. It can be said that Cu element had not enough time to be fully oxidized at this thermal regime. Moreover, $CuAlO_2$ phase also present in the pattern (400ºC) as a result of probable reaction between Cu_2O and Al_2O_3 in the powder mixture. Since Cu_2O phase is oxidized with increasing temperature from 400 to 800ºC, the delafossite and CuO peaks are decreased and increased, respectively. In addition, the peaks of $CuAl_2O_4$ spinel phase (ICDD 01-076-2295) are appeared at 900ºC and are stable up to 1000ºC (Eq. (2)) at this thermal regime. As is obvious from the XRD patterns, the delafossite phase is formed at 1100ºC. However, some small peaks corresponding to $CuAlO_2$ phase are also can be seen in the pattern of 1000ºC. According to the thermodynamic stability phase diagram of Cu-Cu_2O-CuO system (**Fig. 2a**), Cu_2O phase is thermodynamically stable at 1100ºC and air oxygen pressure. On the other hand, DTA analysis confirmed the formation of Cu_2O at around 1020ºC which is consistent with the results presented in other studies [12]. For these reasons, the formed Cu_2O can react with Al_2O_3 forming $CuAlO_2$ phase. Another possible reaction through which the delafossite phase can be produced is Eq. (3).

Fig. 5.

As mentioned before, in-situ XRD was carried out with heating rate of 5ºC/min and 30 minutes stop at some specific temperatures (400, 600, 700, 800, 900, 1000 and 1100ºC) for getting XRD curves (see **Fig. 6a**). Furthermore, corresponding in-situ XRD curves of CH sample as well as XRD pattern of the precursor are provided in **Fig. 6b**. As can be seen, with increasing temperature up to 400ºC, Cu_2O peaks are disappeared and the delafossite peaks are intensified. It can be said that at 400ºC, Cu_2O reacted with alumina and formed $CuAlO_2$ phase, increasing the intensity of the delafossite peaks. It is worth mentioning that with increasing temperature from 400ºC to 800ºC, $CuAlO_2$ phase peaks are getting smaller, and then after, $CuAl_2O_4$ phase is appeared at 900ºC, revealing the decomposition of delafossite and formation of spinel phase through Eq. (3). The same results can be find elsewhere [30,31]. In addition, from 900 to 1100ºC, the amount of spinel phase is increased which can be attributed to the formation of $CuAl_2O_4$ by Eq. (2) [22]. It is worth noting that with

increasing temperature from 1000 to 1100ºC, a peak located at 2-Theta of around 37.5º become larger being attributed to $CuAlO_2$. For better understanding the peak variation of XRD curves, **Fig. 6c** demonstrates the patterns of 1000 and 1100ºC in the range of 36-38º. The literature studies suggest that the reduction of CuO to form Cu_2O phase can take place at temperatures above around 1020ºC [16,17,32]. For this reason, a bulge located at the left-side of the highest intensity peak of $CuAl_2O_4$ in the 1100º XRD pattern of **Fig. 6b** (marked by 1 in **Fig. 6c**) could be attributed to Cu_2O phase. Since the delafossite phase can be produced by Eq. (6), the intensity of $CuAlO_2$ is increased in the mentioned pattern, comparing with lower temperatures (marked by 2 in **Fig. 6c**). Similar observation was also reported by Hu et al [22]. It was said that the disappearance of spinel phase at high temperatures of around 1000ºC is due to the formation of $CuAlO_2$ through the following Eq. (5) and (6). Furthermore, it is also reported that if excess amount of CuO exist in the powder mixture, the delafossite phase could be formed by Eq. (3) with an equilibrium O_2 partial pressure of 0.048 bar [22]. In the present study, the forward reaction is favored because the applied oxygen pressure was around 0.21 bar. It is reported that the much slower rate of spinel decomposition in comparison with CuO phase is likely due to chemical kinetics rather than thermodynamics [22]. Finally, it should be mentioned that the Pt peaks in the XRD patterns of **Fig. 6b** came from the sample holder of the applied XRD instrument.

Fig. 6.

Furthermore, all the precursors were heated from room temperature to 1100ºC and kept for different durations. XRD patterns of the H, CH and F samples after applying heat-treatment at 1100ºC for duration of 1, 3 and 5 hours with corresponding temperature-time graphs are presented in **Fig. 7a-d**. As can be seen in the XRD pattern of H1, all the main peaks correspond to $CuAlO_2$. Moreover, some minor peaks denote CuO phase in the pattern, while all the peaks in H3 and H5 samples are related to delafossite phase. In order to better understand the XRD results, thermodynamic stability phase diagram of Cu-Cu_2O-CuO system is considered (**Fig. 2b**). As is shown in **Fig. 2b**, at temperatures lower than 1050ºC and atmospheric pressure ($\log P_{O2}$=-0.67), CuO is the stable phase. Since the heat-treatment was performed from atmosphere temperature up to 1100ºC and the samples were hold at the target temperature for specific durations (1, 3 and 5 hours), Cu_2O and Cu phases transform to CuO at lower 1050ºC and upper the mentioned temperature, Cu_2O is formed, immediately

reacting with Al_2O_3 to produce $CuAlO_2$. It is worth mentioning that kinetics describes how fast the reaction proceeds from reactants to products. Therefore, it can be said that the duration of 1 hour is not enough for complete formation of delafossite and small amount of CuO can be detected in the corresponding XRD patterns (see **Fig. 7b**, **c** and **d**). Comparing the samples in each group, it can be said that with increasing heating duration from 1 to 5 hours, CuO phase become disappeared. Furthermore, as can be seen in **Fig. 7b** and **d**, duration increment from 1 to 3 h makes $CuAlO_2$ peaks sharper and after that the peaks get smaller (at heat-treatment of 5 h) for both H and F samples. In the case of CH sample (**Fig. 7c**), the intensity of delafossite peaks, first decreased and then increased with increasing time from 1 to 5 hours. The reason for these observations could be attributed to the presence of two eutectic points in $Cu+Cu_2O$ and Cu_2O+CuO systems [36]. Since the eutectic melting points of the mentioned systems are lower than 1100ºC, the eutectic phases may be locally formed, solving $CuAlO_2$ during heat-treatment which results in the reduction of its diffraction peak intensities. However, after 5 hours heat-treatment process, $CuAlO_2$ peaks become stronger again in the case of CH sample.

Fig. 7.

In order to investigate the morphology of the heat-treated powder samples, SEM studies were carried out for F1 sample (**Fig. 8a-d**). According to the SEM image of **Fig. 8a**, three different morphologies can be obviously seen in the microstructure. The marked area in section (a) is provided in **Fig. 8b** at higher magnification showing Al_2O_3 nanomaterials with flaky morphology as also reported elsewhere [34, 35]. It should be said that these nanoflakes were appeared after crystallization by applying heat-treatment, as also reported elsewhere [39]. Moreover, EDS analysis taken from the nano-agglomerated area of Al_2O_3 shows sharp peaks corresponding to aluminum and oxygen (see **Fig. 8b**). It is worth mentioning that Cu peak in the EDS pattern came from Cu containing compounds at the background. Based on the SEM investigations, it was found that the diameter, thickness and aspect ratio of alumina nano-flakes are about 380, 40 and 9.5 nm, respectively. In addition, SEM image of **Fig. 8c** shows $CuAlO_2$ powders together with semi-spherical phases. The regions marked by 1 and 2 are provided at higher magnification in **Fig. 8d**. Comparing the EDS results of **Fig. 8d**, it can be found that phase 1 has small amount of Al, while phase 2 possesses significant amounts of Al and Cu. Combining XRD results (**Fig. 7d**) with EDS analysis, phase 1 and 2 can be attributed

to CuO and $CuAlO_2$, respectively. In addition, as can be seen in **Fig. 8d**, the formed $CuAlO_2$ crystallized in a layered structure being marked by the arrows. It was reported that this layered structure epitaxially growth parallel to Cu-rich planes. **Figure 8e** depicts a unit-cell with rhombohedral configuration in which Cu-rich planes are basal (0003) planes [37-39].

Fig. 8.

Based on the inter-layer spacing calculations, which were done on the SEM images, it was found that the layers have an average separation distance of around 56.186 nm, as is shown in the schematic and SEM images of **Fig. 9**. Moreover, it was reported that the (0001) basal planes (or (0003)) of the $CuAlO_2$ have the intervals of around 0.564 nm. The interval corresponds to one third of the c-axis lattice constant of $CuAlO_2$ [37,38]. Therefore, it can be claimed that the $CuAlO_2$ layers, in the present study, are formed parallel to (0003) planes, because the inter-layer distance (56.186 nm) is approximately hundred folds of the 0.56 nm intervals. These results indicate that $CuAlO_2$ grows epitaxially on its basal planes.

Fig. 9.

Figure 10a, **b** and **c** show SEM micrographs of F sample after treating at 1100ºC for different durations of 1 (F1), 3 (F3) and 5 hours (F5), respectively. As can be seen, with increasing heat-treatment duration from 1 to 5 h, the amount of Al_2O_3 nanoflakes as well as CuO is decreased, while the delafossite phase is increased. This can be attributed to the fact that, with increasing time at high temperature of 1100ºC, CuO phase reduced to Cu_2O and simultaneously reacted with alumina forming $CuAlO_2$ delafossite phase [16,19].

Fig. 10.

Morphology and structure of the prepared powder were also investigated by transmission electron microscopy (TEM) in detail. In this regard, TEM micrographs of CH3 sample are provided in **Fig. 11**. As can be seen, the powders have a flaky-morphology with lamellar structure which is consistent with SEM results. The arrows in the figures show $CuAlO_2$ layers with an average inter-layer spacing of around ~5.7 nm which is approximately ten folds of the basal plane intervals. It is worth noting that this kind of morphology of $CuAlO_2$ was observed for the first time in the present work and, to the best of our knowledge, was not reported elsewhere.

Fig. 11.

3-2-2- Discontinuous heating

As another thermal regime (**Fig. 12a**), H, CH and F samples were directly placed into the furnace at 1100ºC being kept for 30 minutes and air quenched immediately to investigate the formation of $CuAlO_2$. **Figure 12b** shows the XRD results of CH0.5, H0.5 and F0.5 samples. As is obvious, all the peaks correspond to the delafossite phase confirming the formation of $CuAlO_2$ just after 30 minutes heat-treatment. However, a small peak in CH0.5 sample was denoted as alumina phase and the presence of Al_2O_3 is further confirmed in the microstructure by inset SEM image of **Fig. 12b**. Furthermore, in order to study the morphology of the formed delafossite after applying 30 minutes heating, SEM images of H0.5, F0.5 and CH0.5 samples are presented in **Fig. 12c**, **d** and **e**, respectively. As is obvious, the lamellar structure of $CuAlO_2$ can be clearly seen in the magnified SEM micrographs of all three samples (**Fig. 12c-e**).

Fig. 12.

To better understand the effect of discontinuous heating on the crystallization of $CuAlO_2$, this thermal regime was applied at different temperatures (400, 600, 700, 800, 900, 1000 and 1100ºC) for CH sample as demonstrated in the schematic of **Fig. 13a**. **Figure 13b** shows the XRD patterns which were obtained after heat-treatment at different target temperatures. Moreover, XRD pattern of CH precursor is also shown in **Fig. 13b** in order to better understand the peaks evolution. As can be seen in **Fig. 13b**, Cu peaks intensities significantly become smaller at 400ºC because of enough duration for Cu_2O and CuO to be formed (in comparison with continuous condition). In the temperature range of 600-800ºC, CuO phase is thermodynamically stable which can be confirmed by the XRD results. However, at 900ºC, CuO reacted with alumina making spinel phase ($CuAl_2O_4$) appear. Above the mentioned temperature, i.e. 1000ºC, which is highly close to the reduction temperature of CuO (1020ºC), the formed Cu_2O is reacted with Al_2O_3 resulting in the formation of $CuAlO_2$ phase. Nevertheless, CuO peaks still present in the XRD pattern of 1000ºC which reveals that the time for completion the of Eq. (4) was not enough. As is obvious, at the temperature of 1100ºC, all peaks correspond to delafossite phase. At this temperature, the formation of Cu_2O is kinetically favorable, and therefore, the formation of $CuAlO_2$ is facilitated through Eq. (6). However, a small amount of spinel phase might be formed at this temperature which could not be detected by XRD analysis. Moreover, TEM images of **Fig. 14**, which belongs to

CH0.5 sample, again reveals the lamellar structure of the powders with approximately the same intervals as before (~5.7 nm).

Fig. 13

Fig. 14.

3-3- One-step process: SCS

Considering the XRD results of the discontinuous heat-treated samples, the delafossite main peaks can be obviously seen at a temperature of 1000°C (**Fig. 13b**). In this regard, solution combustion process was performed at higher temperatures of 1000, 1100, 1200 and 1250ºC, instead of 300 and 500ºC. **Figure 15a** shows the XRD patterns of the combustion synthesized samples at the mentioned temperatures. Based on the patterns, it can be said that the delafossite phase is crystallized through the one-step solution combustion at 1000ºC. However, some peaks corresponding to alumina and CuO phases can also be detected in the pattern without any sign of Cu_2O and Cu presence. Therefore, $CuAlO_2$ phase may be produced directly from the reaction between Cu_2O and Al_2O_3 during the one-step process. Moreover, comparing the XRD patterns reveals that the intensity of $CuAlO_2$ peaks is increased being attributed to the higher formation of Cu_2O phase which reacts with alumina and finally forms higher amount of delafossite phase with increasing temperature from 1000 to 1250ºC. In addition, with increasing temperature from 1100 to 1200°C, Al_2O_3 peaks become disappeared while the intensity of CuO and $CuAlO_2$ peaks is decreased and increased, respectively. Finally, delafossite peaks are dominant in the corresponding XRD pattern after applying a one-step combustion synthesis without controlling the atmosphere at 1250ºC. **Figure 15b** demonstrates the SEM micrographs of the powder sample synthesized at 1250ºC. As is obvious, the sample has a 3D hierarchical porous structure which includes the pores having mean size of ~9 μm with the pore walls possessing numerous sub-micropores with a size range of ~300-800 nm. The achieved porous structure can be attributed to the rapid release of the gases products during the combustion synthesis [16]. The produced porous sample and its application in biomedical fields will be explored in the future studies in detail. Variation of adiabatic temperature as a function of initial applied temperature is illustrated in **Fig15c**. With increasing initial temperature, the adiabatic temperature is

increased theoretically. According to the XRD results of **Fig2a**, initial temperature has a main effect on the resultant product after combustion. In addition, the powder morphology of the solution combustion synthesized sample at 1250ºC was also investigated by TEM and the corresponding micrographs are presented in **Fig. 16**. As is obvious, the powders have a flaky-morphology with lamellar structure. Furthermore, the arrows in **Fig. 16a** show $CuAlO_2$ layers with an average inter-layer spacing of around ~5.8 nm which again is approximately ten folds of the basal plane intervals. Finally, it can be said that $CuAlO_2$ phase was successfully obtained through a one-step combustion synthesis for the first time.

Fig. 15.

Fig. 16.

4- Summary

To sum up, two different processes (one-step vs two-step) were applied to produce $CuAlO_2$ powder sample. As a one-step process, SCS was used at different temperatures. On the other hand, as a two-step process, SCS followed by continuous and discontinuous heat-treatment were applied. Furthermore, in-situ XRD was also used to investigate the evolution of phase composition during continuous heating. based on the in-situ XRD tests (heating at 5ºC/min) which lasted around 8 hours, it can be said that the mentioned prolonged time kinetically satisfied the formation of spinel phase. However, the spinel phase was not detected in DTA/continuous heating (heating at 5ºC/min) which lasted around 3 hours, because the nucleation of $CuAl_2O_4$ is so slow and kinetically need an appropriate duration [43]. It was also reported that the rates of spinel formation decrease in the sequence of $ZnAl_2O_4$>$MgAl_2O_4$>$CuAl_2O_4$ [44]. Furthermore, regarding the spinel phase decomposition in the applied in-situ XRD the following points should be stated. $CuAl_2O_4$ has high thermal stability and will decompose at almost high temperatures or high durations [45]. Therefore, the formation of $CuAlO_2$ delafossite is postponed to higher temperatures/durations. When the precursors containing Cu_2O/Cu directly experience 1100ºC for 30 minutes (**Fig. 12b**), the final phase is delafossite, because in the mentioned temperature Cu_2O phase is stable reacting with alumina to form $CuAlO_2$. It can be said that the heat-treatment time duration needed for the crystallization of $CuAlO_2$ was lowered to 30 minutes at 1100ºC by exerting SCS on the mixture of starting materials, because it was reported that without applying SCS, delafossite phase was achieved by heat treating of Cu_2O/Al_2O_3 powder mixture at 1100ºC after a long

duration of 20 hours [10]. However, when the heating was applied continuously from room temperature up to 1100ºC and the sample was held for 1 hour, Cu and Cu_2O phases were oxidized forming CuO. Since the formation of $CuAlO_2$ is happened through the reacting between Cu_2O and alumina, therefore, the duration of continuous thermal regime may not be enough to fully form Cu_2O from CuO, and some small peaks still exist in the XRD pattern (see **Fig. 7b-d**). Briefly, it was revealed that different thermal regimes affect the crystallization of $CuAlO_2$ because the samples experienced different durations up to 1100ºC. At discontinuous thermal regime in which the sample experienced a short duration, $CuAlO_2$ phase was formed at 1000ºC (**Fig. 13b**). While, in the in-situ XRD test, the final phase at 1100ºC was $CuAl_2O_4$ and the delafossite phase may be formed at higher temperatures/higher durations. Based on the XRD results of different thermal regimes, it can be said that at higher durations (3 and 8 hours) of in-situ XRD and continuous heating, spinel phase could be formed and stable at higher temperatures postponing the delafossite phase formation. However, discontinuous heating at 1100ºC prevent the formation of spinel phase. Hence, it can be concluded that decreasing the duration of heat-treatment and preventing the formation of spinel phase are favorable for the formation of delafossite $CuAlO_2$. As mentioned before, high temperature and very short duration can be achieved by SCS process because of its rapid nature and for the mentioned reasons $CuAlO_2$ was successfully synthesized through a one-step SCS process. It should be mentioned that the produced delafossite phase in the present study had a flaky-shape morphology with lamellar structure.

5- Conclusions

In this study, $CuAlO_2$ was successfully produced via a one-step process, namely solution combustion synthesis (SCS). In addition, delafossite $CuAlO_2$ phase was also successfully synthesized using SCS followed by heat-treatment (two-step process) in order to accelerate $CuAlO_2$ crystallization. The powder precursor was prepared from copper and aluminum nitrate together with hexamine at three different conditions as follows: (i) on 300ºC hot-plate/open system, (ii) on 300ºC hot-plate/closed-system (producing low oxygen partial pressure), and (iii) in 500ºC furnace. After preparing the precursors (SCS), heat-treatment with different thermal regimes (continuous and discontinuous heating) was applied in order to produce a single-phase $CuAlO_2$ (two-step process). As a one-step process, SCS was performed on the before-prepared solutions in the furnace with temperatures of 1000, 1100,

1200 and 1250ºC. Composition, microstructure and morphology of the produced powders were studied by XRD, in-situ XRD, SEM and TEM. According to the in-situ XRD test performed from room temperature up to 1100ºC, it was found that the formed delafossite phase decomposed in the range of 400-800ºC, and then, the $CuAl_2O_4$ spinel phase became appeared. However, at 1100ºC, a small amount of $CuAlO_2$ was found in the pattern being attributed to the decomposition of $CuAl_2O_4$ spinel phase. In discontinuous heating, it was revealed that the mentioned condition was suitable for delafossite phase to be achieved. Moreover, it was found that when the precursors containing Cu_2O/Cu phases directly placed at 1100ºC for 30 minutes, the final phase is delafossite. However, when the heating was applied continuously from room temperature up to 1100ºC and kept for 1 hour, Cu as well as Cu_2O phases were oxidized producing CuO. The time needed for continuous thermal regime was not enough to fully form Cu_2O, and therefore, CuO phase was observed together with $CuAlO_2$. Moreover, in the one-step SCS, delafossite peaks were dominant in the corresponding XRD pattern after applying combustion synthesis atmosphere at 1250ºC. Furthermore, SEM and TEM studies revealed a lamellar structure of $CuAlO_2$ powder sample which was formed parallel to the delafossite basal planes (0003). Finally, it can be said that one of the main challenges in the formation of $CuAlO_2$, i.e. high operation time to be needed for producing delafossite phase, was solved in this study. The present findings may open up a window to the new area in which other delafossite materials such as $CuCrO_2$, $CuAgO_2$, $CuScO_2$ and so on can be produced.

References

[1] H. Kawazoe, M. Yasukawa, H. Hyodo, M. Kurita, H. Yanagi, H. Hosono, P-type electrical conduction in transparent thin films of $CuAlO_2$, Nature. 389 (1997) 939–942. https://doi.org/10.1038/40087.

[2] A. Kudo, H. Yanagi, H. Hosono, H. Kawazoe, $SrCu_2O_2$: A p-type conductive oxide with wide band gap, Appl. Phys. Lett. 73 (1998) 220–222. https://doi.org/10.1063/1.121761.

[3] H. Hiramatsu, K. Ueda, H. Ohta, T. Kamiya, M. Hirano, H. Hosono, Excitonic blue luminescence from p-LaCuOSen-InGa Zn5 O8 light-emitting diode at room temperature, Appl. Phys. Lett. 87 (2005) 1–3. https://doi.org/10.1063/1.2133907.

[4] Y.R. Ryu, S. Zhu, D.C. Look, J.M. Wrobel, H.M. Jeong, H.W. White, Synthesis of p-type ZnO films, J. Cryst. Growth. 216 (2000) 330–334. https://doi.org/10.1016/S0022-0248(00)00437-1.

[5] C.H. Shih, B.H. Tseng, Formation Mechanism of CuAlO2 Prepared by Rapid Thermal Annealing of Al_2O_3/Cu_2O/Sapphire Sandwich Structure, Phys. Procedia. 32 (2012) 395–400. https://doi.org/10.1016/j.phpro.2012.03.574.

[6] X.G. Zheng, K. Taniguchi, A. Takahashi, Y. Liu, C.N. Xu, Room temperature sensing of ozone by transparent p-type semiconductor $CuAlO_2$, Appl. Phys. Lett. 85 (2004) 1728–1729. https://doi.org/10.1063/1.1784888.

[7] J. Ahmed, C.K. Blakely, J. Prakash, S.R. Bruno, M. Yu, Y. Wu, V. V. Poltavets, Scalable synthesis of delafossite $CuAlO_2$ nanoparticles for p-type dye-sensitized solar cells applications, J. Alloys Compd. 591 (2014) 275–279.

https://doi.org/10.1016/j.jallcom.2013.12.199.

[8] C.K. Ghosh, S.R. Popuri, T.U. Mahesh, K.K. Chattopadhyay, Preparation of nanocrystalline CuAlO2 through sol-gel route, J. Sol-Gel Sci. Technol. 52 (2009) 75–81. https://doi.org/10.1007/s10971-009-1999-x.

[9] N. Benreguia, A. Barnabé, M. Trari, Sol–gel synthesis and characterization of the delafossite $CuAlO_2$, J. Sol-Gel Sci. Technol. 75 (2015) 670–679. https://doi.org/10.1007/s10971-015-3737-x.

[10] T. Prakash, K.P. Prasad, S. Ramasamy, B.S. Murty, Optical and electrical properties of mechanochemically synthesized nanocrystalline delafossite $CuAlO_2$, J. Nanosci. Nanotechnol. 8 (2008) 4273–4278. https://doi.org/10.1166/jnn.2008.AN23.

[11] D. Xiong, X. Zeng, W. Zhang, H. Wang, X. Zhao, W. Chen, Synthesis and Characterization of $CuAlO_2$ and $AgAlO_2$ Delafossite Oxides through Low-Temperature Hydrothermal Methods, (2014).

[12] K. Vojisavljević, B. Malič, M. Senna, S. Drnovšek, M. Kosec, Solid state synthesis of nano-boehmite-derived CuAlO2 powder and processing of the ceramics, J. Eur. Ceram. Soc. 33 (2013) 3231–3241. https://doi.org/10.1016/j.jeurceramsoc.2013.05.025.

[13] T. Ehara, R. Iizaka, M. Abe, K. Abe, T. Sato, Preparation of $CuAlO_2$ thin films by radio frequency magnetron sputtering and the effect of sputtering on the target surface, J. Ceram. Sci. Technol. 8 (2017) 7–12. https://doi.org/10.4416/JCST2016-00066.

[14] S. Agrawal, A. Parveen, A. Azam, Influence of Mg on structural, electrical and magnetic properties of $CuAlO_2$ nanoparticles, Mater. Lett. 168 (2016) 125–128. https://doi.org/10.1016/j.matlet.2016.01.046.

[15] Y. Wang, C. Dong, Y. Chuai, Y. Wang, Room temperature ferromagnetism in Co-doped $CuAlO_2$ nanofibers fabricated by electrospinning, J. Wuhan Univ. Technol. Mater. Sci. Ed. 30 (2015) 1–5. https://doi.org/10.1007/s11595-015-1089-6.

[16] H. Aali, N. Azizi, N. Javadi Baygi, F. Kermani, M. Mashreghi, A. Youssefi, S. Mollazadeh, J.V. Khaki, H. Nasiri, High antibacterial and photocatalytic activity of solution combustion synthesized $Ni_{0.5}Zn_{0.5}Fe_2O_4$ nanoparticles: Effect of fuel to oxidizer

ratio and complex fuels, Ceram. Int. 45 (2019) 19127–19140. https://doi.org/10.1016/j.ceramint.2019.06.159.

[17] N.J. Baygi, A.V. Saghir, S.M. Beidokhti, J.V. Khaki, Modified auto-combustion synthesis of mixed-oxides TiO2/NiO nanoparticles: Physical properties and photocatalytic performance, Ceram. Int. (2020). https://doi.org/10.1016/j.ceramint.2020.03.087.

[18] F. Kermani, A. Gharavian, S. Mollazadeh, S. Kargozar, A. Youssefi, J. Vahdati Khaki, Silicon-doped calcium phosphates; the critical effect of synthesis routes on the biological performance, Elsevier B.V, 2020. https://doi.org/10.1016/j.msec.2020.110828.

[19] H. Kazemi, F. Kermani, S. Mollazadeh, J. Vahdati Khakhi, The Significant Role of the Glycine-Nitrate Ratio on the Physicochemical Properties of $Co_xZn_{1-x}O$ Nanoparticles , 2020. https://doi.org/10.1111/ijac.13515.

[20] K.B. Podbolotov, A.A. Khort, A.B. Tarasov, G. V. Trusov, S.I. Roslyakov, A.S. Mukasyan, Solution Combustion Synthesis of Copper Nanopowders: The Fuel Effect, Combust. Sci. Technol. 189 (2017) 1878–1890. https://doi.org/10.1080/00102202.2017.1334646.

[21] R.A. Adams, V.G. Pol, A. Varma, Tailored Solution Combustion Synthesis of High Performance ZnCo2O4 Anode Materials for Lithium-Ion Batteries, Ind. Eng. Chem. Res. 56 (2017) 7173–7183. https://doi.org/10.1021/acs.iecr.7b00295.

[22] W. Hu, F. Donat, S.A. Scott, J.S. Dennis, RSC Advances The interaction between CuO and Al 2 O 3 and the reactivity of copper aluminates below 1000 C and their implication on the use of the Cu – Al – O system for oxygen storage and production †, RSC Adv. 6 (2016) 113016–113024. https://doi.org/10.1039/C6RA22712K.

[23] K.T. Jacob, C.B. Alcock, in the System Cu20Xu0-Al2O3, (1974) 192–195.

[24] J. Wang, A. Hu, J. Persic, J.Z. Wen, Y.N. Zhou, Thermal stability and reaction properties of passivated, J. Phys. Chem. Solids 72 (2011) 620–625. https://doi.org/10.1016/j.jpcs.2011.02.006.

[25] N.M. Deraz, Structural and Morphological Characteristics of Copper- Alumina Nano-Composite, 8 (2013) 5213–5222.

[26] H. Aali, S. Mollazadeh, J.V. Khaki, Quantitative evaluation of ambient O_2 interference during solution combustion synthesis process:considering iron nitrate – fuel system, Ceram. Int. (2019) 0–1. https://doi.org/10.1016/j.ceramint.2019.05.348.

[27] F. Kermani, S. Mollazadeh, J. Vahdati Khaki, A simple thermodynamics model for estimation and comparison the concentration of oxygen vacancies generated in oxide powders synthesized via the solution combustion method, Ceram. Int. 45 (2019) 13496–13501. https://doi.org/10.1016/j.ceramint.2019.04.053.

[28] H. Aali, S. Mollazadeh, J.V. Khaki, Single-phase magnetite with high saturation magnetization synthesized via modified solution combustion synthesis procedure, Ceram. Int. 44 (2018) 20267–20274. https://doi.org/10.1016/j.ceramint.2018.08.012.

[29] F. Nishino, M. Jeem, L. Zhang, K. Okamoto, S. Okabe, S. Watanabe, Formation of CuO nano-flowered surfaces via submerged photo-synthesis of crystallites and their antimicrobial activity, Sci. Rep. 7 (2017) 1–11. https://doi.org/10.1038/s41598-017-01194-5.

[30] Ž.D. Živković, D.T. Živković, D.B. Grujičić, Kinetics and mechanism of the thermal decomposition of M(NO3)2·nH2O (M=Cu, Co, Ni), J. Therm. Anal. Calorim. 53 (1998) 617–623. https://doi.org/10.1023/A:1010170231923.

[31] S.P. Patil, S.P. Patil, V.R. Puri, L.D. Jadhav, Synthesis and characterization of pure Cu and CuO nano particles by solution combustion synthesis, AIP Conf. Proc. 1536 (2013) 1260–1261. https://doi.org/10.1063/1.4810699.

[32] K.C. Song, K.J. Woo, Y. Kang, Preparation of alumina fibers from aluminum salts by the sol-gel method, Korean J. Chem. Eng. 16 (1999) 75–81. https://doi.org/10.1007/BF02699008.

[33] J.C. Lee, S.Y. Um, Y.W. Heo, J.H. Lee, J.J. Kim, Phase development and crystallization of CuAlO2 thin films prepared by pulsed laser deposition, J. Eur. Ceram. Soc. 30 (2010) 509–512. https://doi.org/10.1016/j.jeurceramsoc.2009.05.025.

[34] C. Scheu, S. Klein, A.P. Tomsia, M. Rühle, Chemical reactions and morphological stability at the Cu/Al_2O_3 interface, J. Microsc. 208 (2002) 11–17.

https://doi.org/10.1046/j.1365-2818.2002.01065.x.

[35] D.Y. Shahriari, A. Barnabe, T.O. Mason, K.R. Poeppelmeier, A High-Yield Hydrothermal Preparation of CuAlO 2, (2001) 5734–5735.

[36] B. Ma, M. Zhu, M. Zheng, Y. Hou, Improvement in electrical properties of thermoelectric CuAlO 2 ceramics aided by aluminosilicate glass, Int. J. Appl. Ceram. Technol. 15 (2018) 1301–1309. https://doi.org/10.1111/ijac.12890.

[37] S.G. Shabestari, THERMOCHEMICAL SYNTHESIS OF NANOSTRUCTURED Cu-Al_2O_3 COMPOSITE, 20 (2014) 339–344. https://doi.org/10.2298/CICEQ120702015S.

[38] Y. Lu, K. Maeda, K. Sagara, L. Hao, Y. Jin, Improvement of thermoelectric properties of CuAlo2 by excess oxygen doping in annealing, Mater. Sci. Forum. 750 (2013) 134–137. https://doi.org/10.4028/www.scientific.net/MSF.750.134.

[39] T. Sato, K. Sue, H. Tsumatori, M. Suzuki, S. Tanaka, A. Kawai-Nakamura, K. Saitoh, K. Aida, T. Hiaki, Hydrothermal synthesis of $CuAlO_2$ with the delafossite structure in supercritical water, J. Supercrit. Fluids. 46 (2008) 173–177. https://doi.org/10.1016/j.supflu.2008.04.002.

[40] H. Tajizadegan, O. Torabi, A. Heidary, M.H. Golabgir, F. Siampour, Influence of Different Alumina Precursors on Structural Properties and Morphology of ZnO-Al_2O_3 Nanocomposite Powder, Int. J. Appl. Ceram. Technol. 12 (2015) E162–E169. https://doi.org/10.1111/ijac.12388.

[41] J. Lian, J. Ma, X. Duan, T. Kim, H. Li, W. Zheng, One-step ionothermal synthesis of γ-Al2O3 mesoporous nanoflakes at low temperature, Chem. Commun. 46 (2010) 2650–2652. https://doi.org/10.1039/b921787h.

[42] Z. Yu, M. Kracum, A. Kundu, M.P. Harmer, H.M. Chan, Microstructural Evolution of a Cu and θ-Al_2O_3 Composite Formed By Reduction of Delafossite $CuAlO_2$: A HAADF-STEM Study, Cryst. Growth Des. 16 (2016) 380–385. https://doi.org/10.1021/acs.cgd.5b01362.

[43] M. Arjmand, A.M. Azad, H. Leion, T. Mattisson, A. Lyngfelt, Evaluation of $CuAl_2O_4$ as an oxygen carrier in chemical-looping combustion, Ind. Eng. Chem. Res. 51 (2012)

13924–13934. https://doi.org/10.1021/ie300427w.

[44] S.G. Menon, S.D. Kulkarni, K.S. Choudhari, C. Santhosh, Diffusion-controlled growth of $CuAl_2O_4$ nanoparticles: effect of sintering and photodegradation of methyl orange, J. Exp. Nanosci. 11 (2016) 1227–1241. https://doi.org/10.1080/17458080.2016.1209585.

[45] X. Guo, P. Yin, W. Lei, H. Yang, Preparation of a macroporous $CuAl_2O_4$ spinel monolith and its rapid selective adsorption towards some anionic dyes, New J. Chem. 41 (2017) 11998–12005. https://doi.org/10.1039/c7nj02279d.

Table 1. A summary of the reactions 1-6 including reactants, intermediate phases and final products.

Reactants	Intermediate phases		Final products	References
Cu_2O, Al_2O_3	CuO, Al_2O_3 (200ºC-500ºC)	$CuAl_2O_4$, CuO (<1100ºC)	$CuAlO_2$ (1100ºC)	[22]
CuO, Al_2O_3	Cu_2O, $CuAl_2O_4$ (1020ºC)		$CuAlO_2$ (1100ºC)	[12]
Al, CuO	Cu_2O, Al_2O_3 (570ºC)		$CuAlO_2$ (>800ºC)	[24]

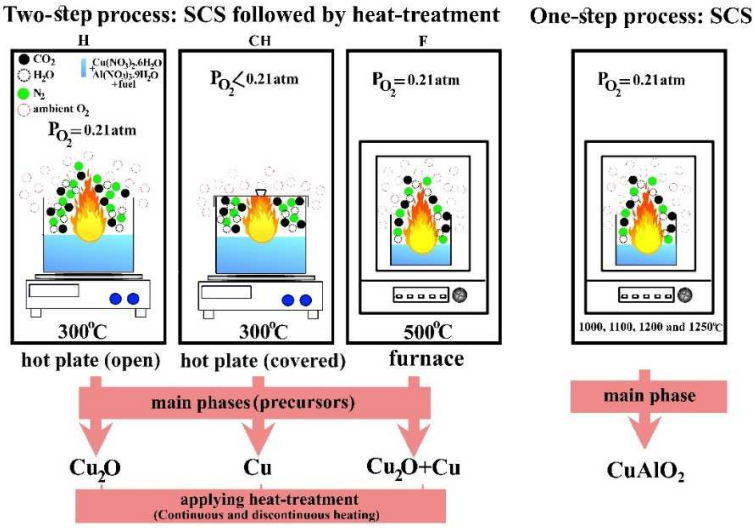

Fig. 1. Schematic illustration of the applied procedures including one-step and two-step processes.

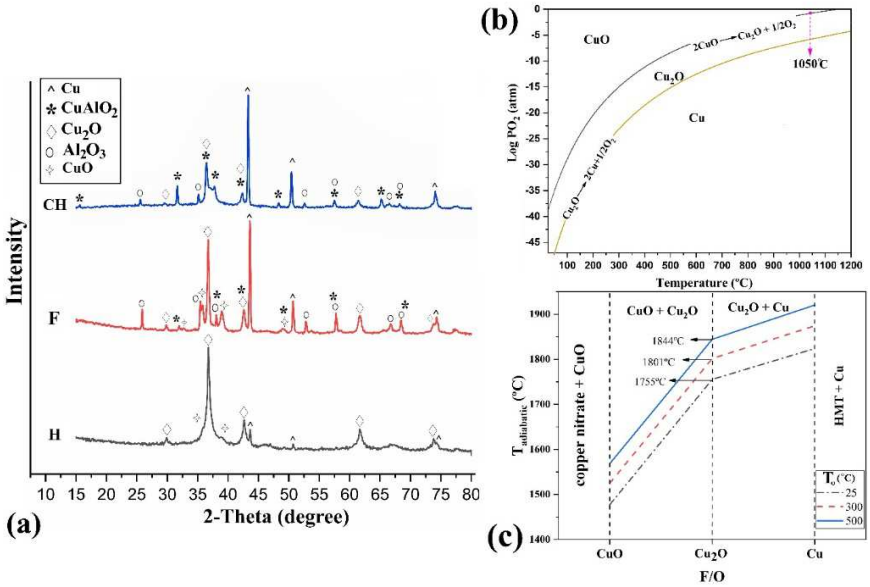

Fig.2. (a) XRD patterns of the prepared precursors at different conditions of H, CH and F. (b) Stable phases in Cu–O system as a function of temperature and oxygen partial pressure. (c) Variation of adiabatic temperature as a function of fuel to oxidizer ratio (F/O) at different initial temperatures (T_o).

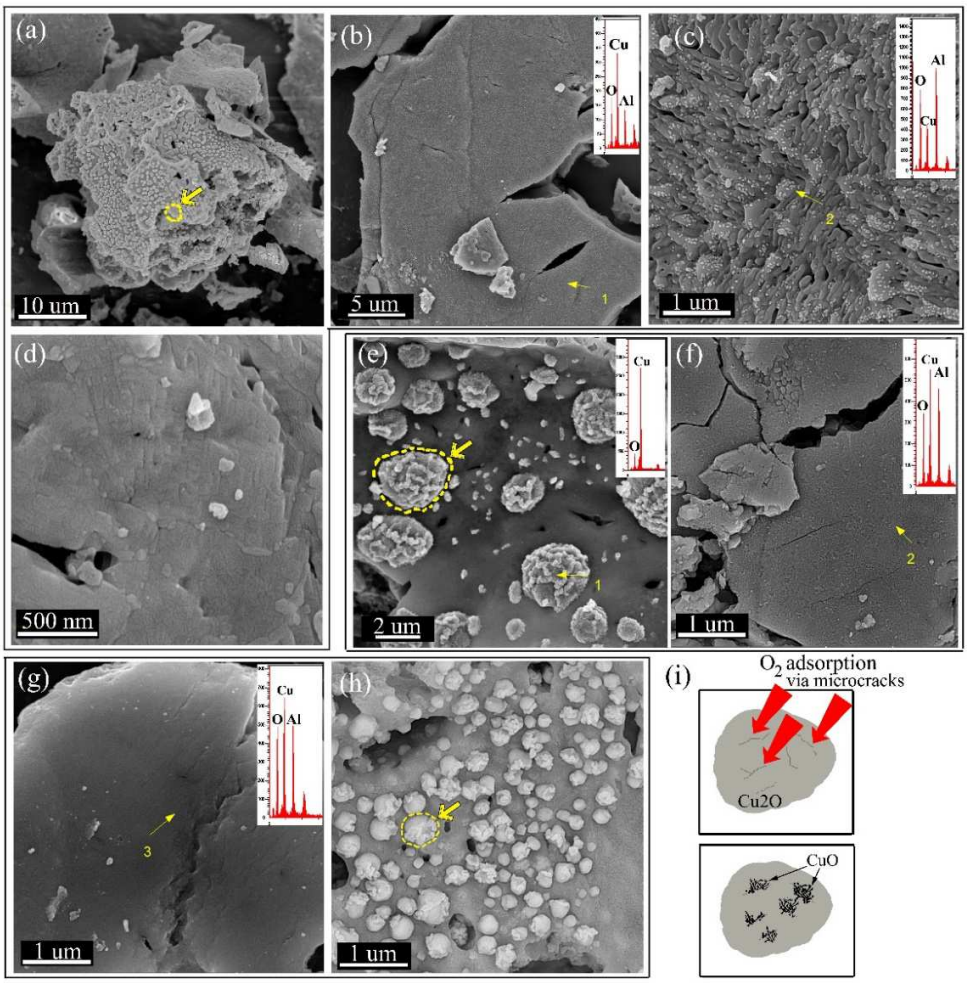

Fig. 3. FESEM micrographs of CH (a-d), F (e-f) and H (g-h) precursors. (i) Schematic illustration of Cu_2O oxidation.

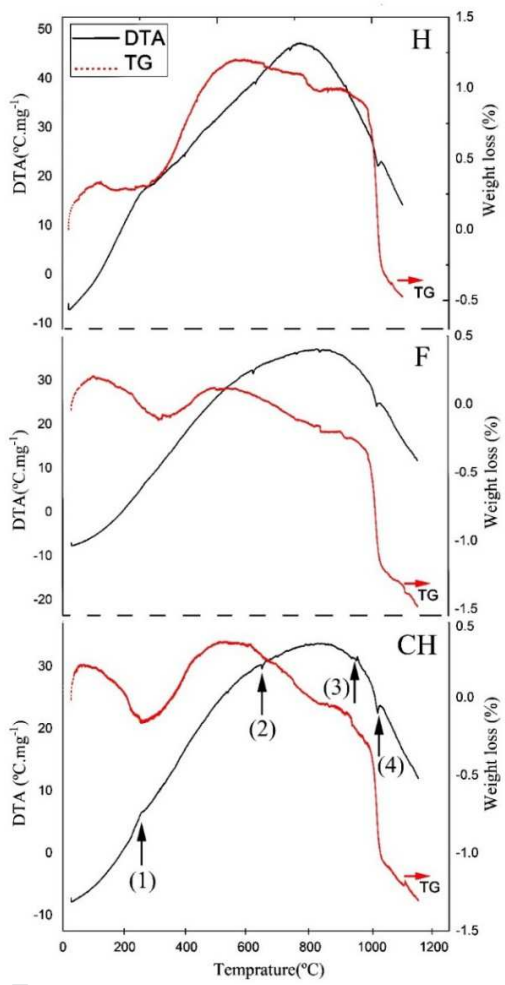

Fig. 4. DTA/TG curves of H (a), F (b), CH (c) powder samples.

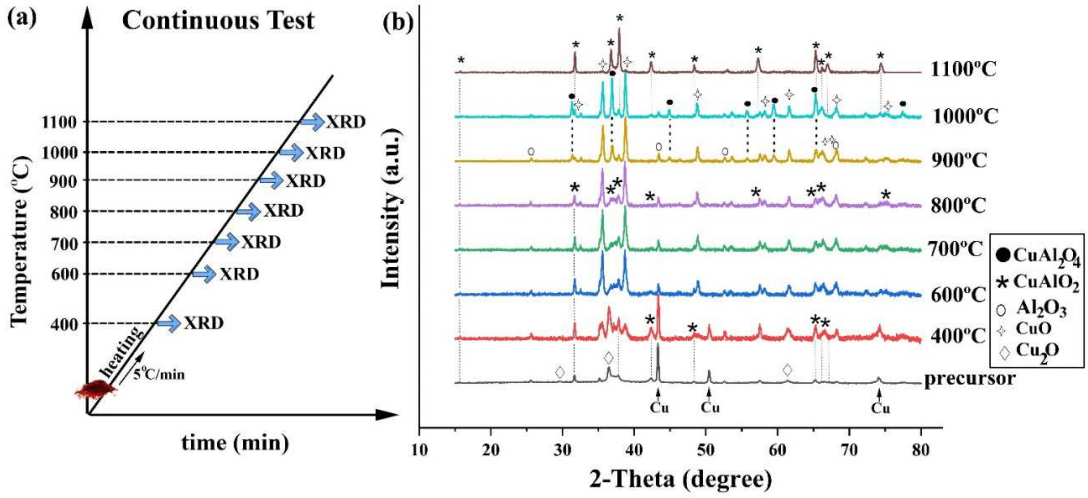

Fig. 5. Continuous thermal regime: (a) Temperature-time graph, and (b) XRD patterns of CH sample at different temperatures.

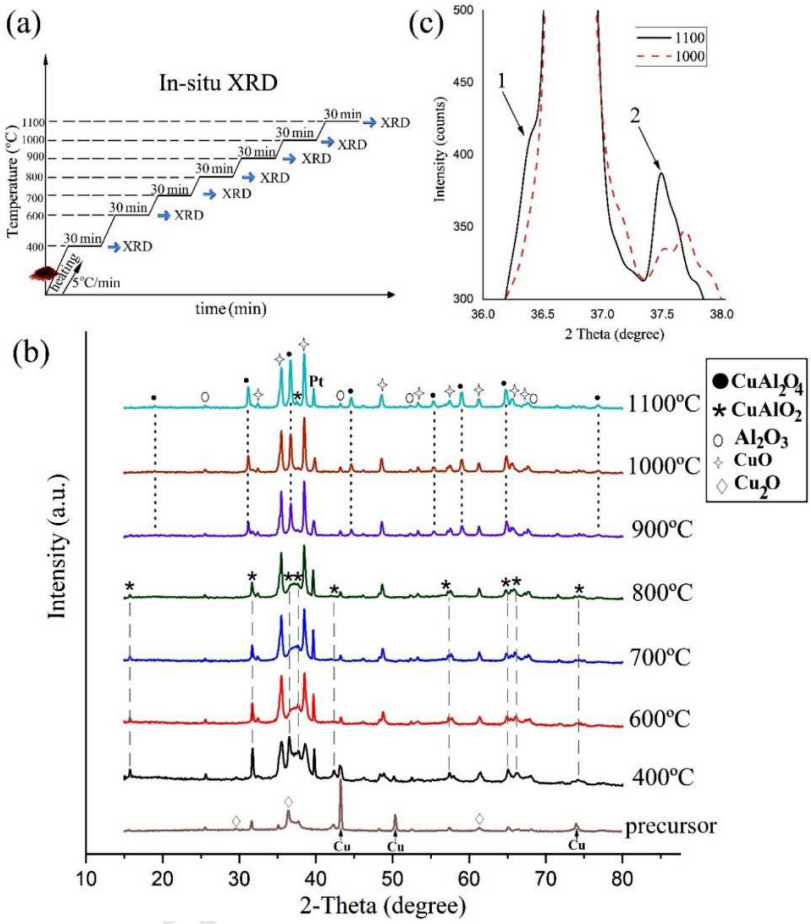

Fig. 6. (a) Temperature-time graph for in-situ XRD, (b) In-situ XRD patterns of CH sample as well as precursor and (c) XRD patterns of 1000 and 1100ºC in the range of 36-38º.

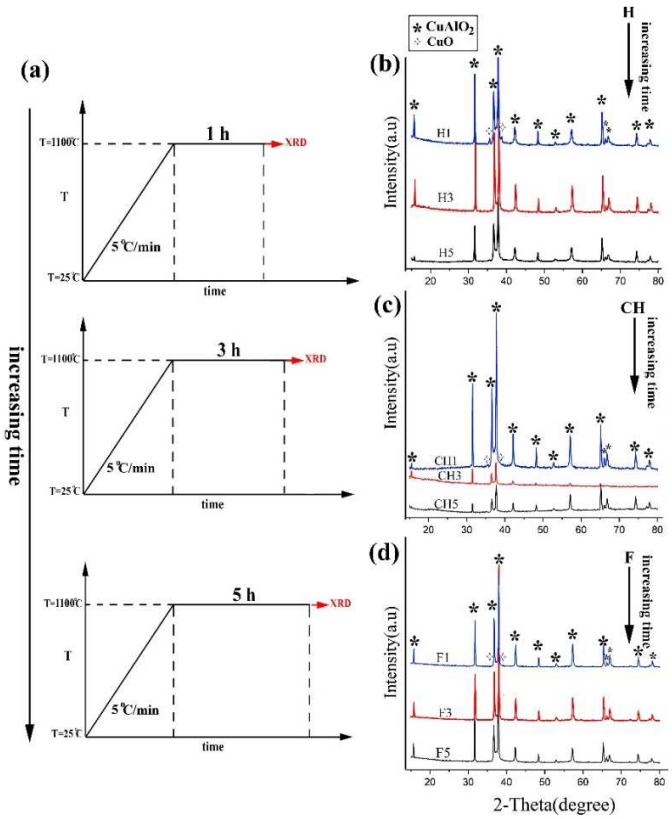

Fig. 7. (a) Temperature-time graphs for the applied heat-treatment processes, XRD patterns for H (b), CH (c) and F (d) samples after applying heat-treatment for 1, 3 and 5 hours.

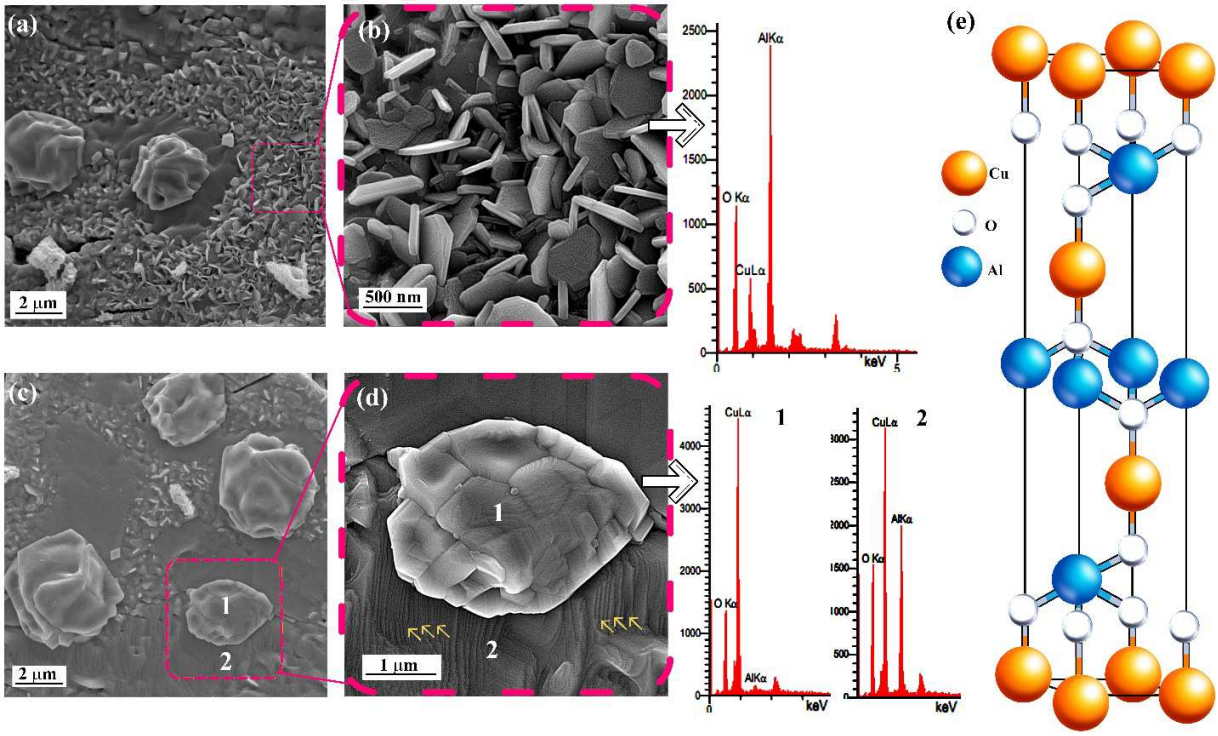

Fig. 8. (a-d) FESEM micrographs of F1 sample showing different morphologies: (a) agglomeration of nano-Alumina at lower magnification with corresponding higher magnification SEM image (b) and related EDS analysis. (e) a unit-cell with rhombohedral configuration.

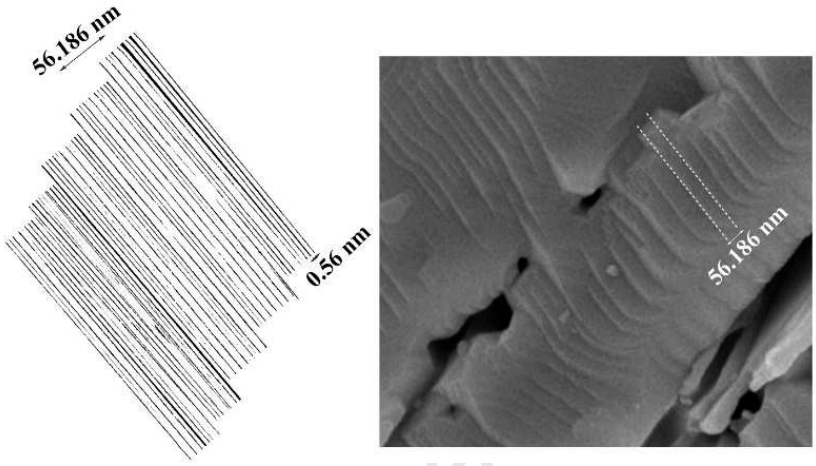

Fig. 9. Representative SEM image together with the corresponding schematic showing the intervals between basal planes.

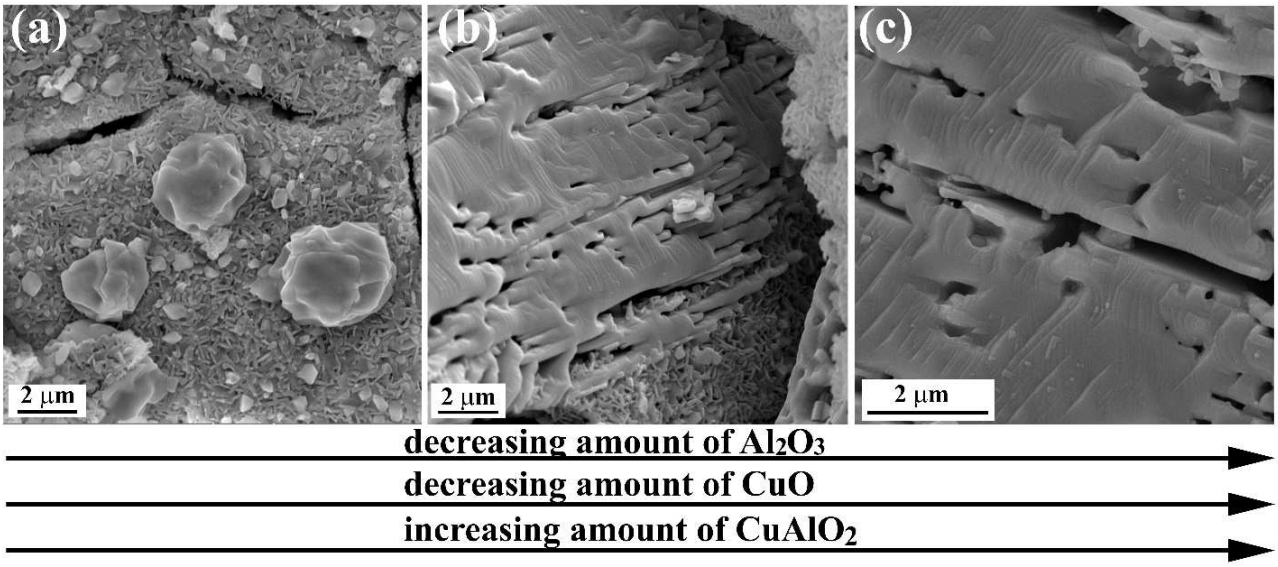

Fig. 10. FESEM micrographs of F1 (a), F3 (b) and F5 (c) samples after heat-treatment at 1100ºC.

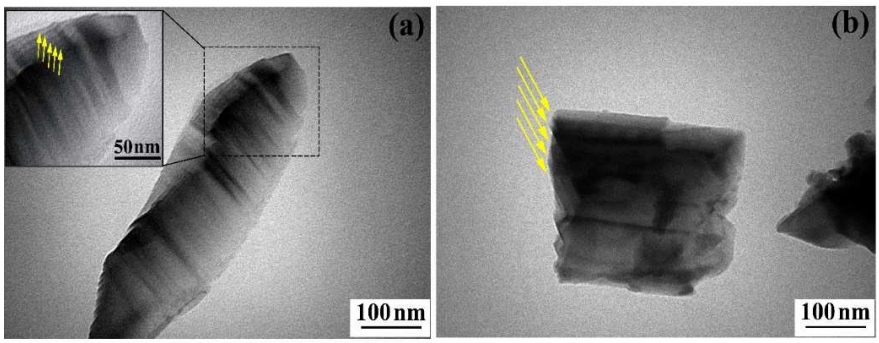

Fig. 11. (a, b) TEM micrographs of CH3 powder sample showing flaky-morphology.

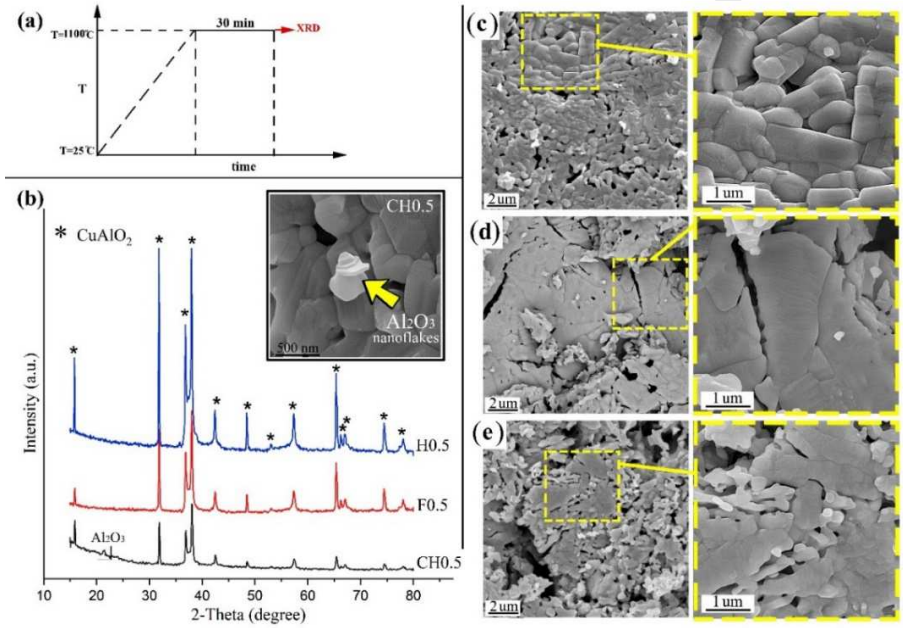

Fig. 12. Discontinuous thermal regime: (a) Temperature-time graph for 30 minutes heat-treatment at 1100ºC and (b) XRD patterns of H0.5, F0.5 and CH0.5 samples. The inset shows alumina nanoflakes. FESEM micrographs of H0.5 (c), F0.5 (d) and CH0.5 (e) samples.

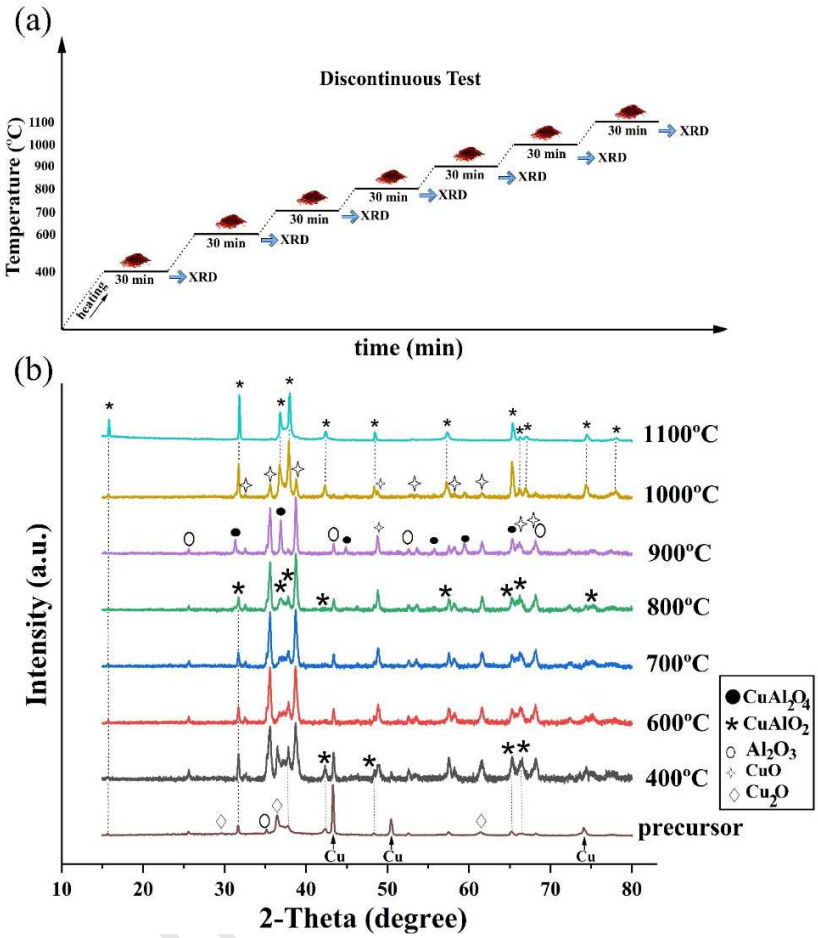

Fig. 13. (a) Temperature-time graph for discontinuous heat-treatment and (b) XRD patterns of CH sample.

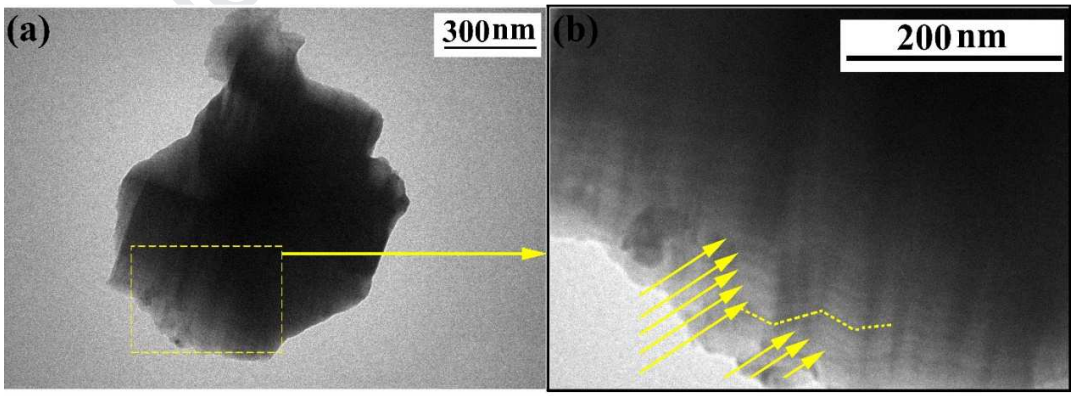

Fig. 14. TEM micrographs of CH0.5 powder sample showing flaky-morphology with lamellar structure (marked by arrows in section b).

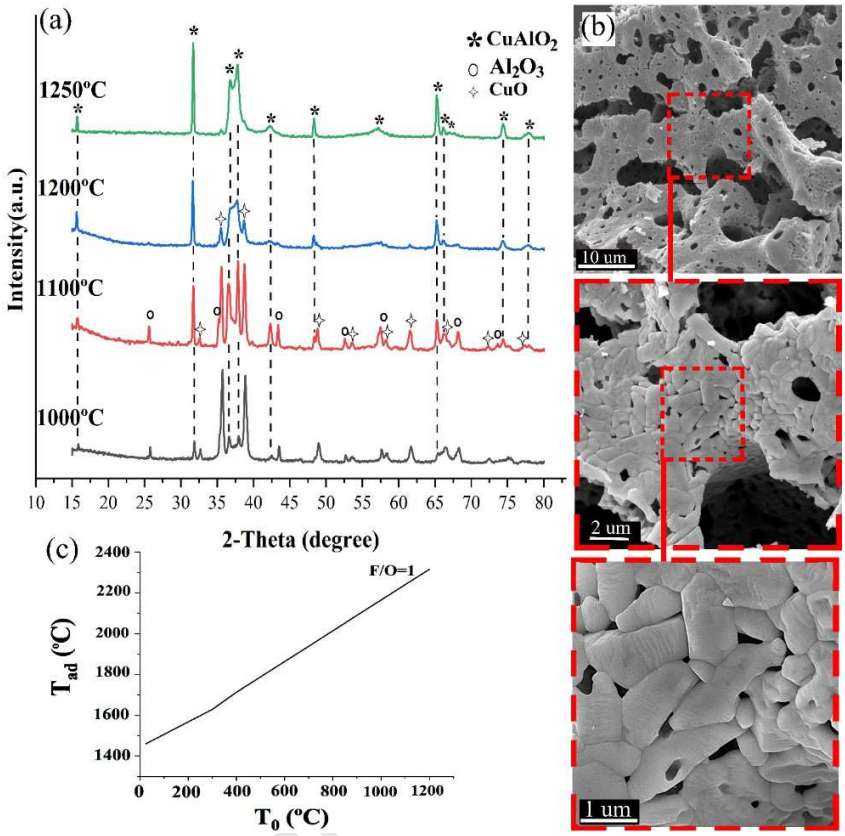

Fig. 15. (a) XRD patterns of the samples after one-step SCS at different temperatures, (b) FESEM micrographs of the as synthesized sample after applying SCS at 1250ºC and (c) Variation of adiabatic temperature as a function of initial applied temperature for F/O=1.

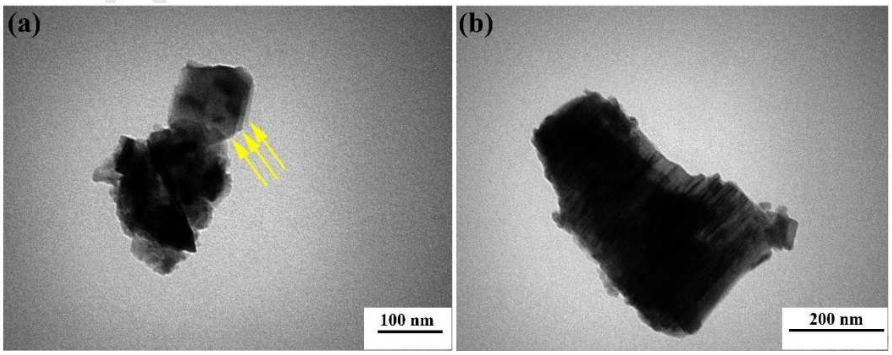

Fig. 16. (a, b) TEM micrographs of the as synthesized powder sample after one-step SCS at 1250ºC.

Accelerated crystallization of $CuAlO_2$ delafossite phase by controlling thermal regime during solution combustion synthesis

Elham Garmroudi Nezhad, Sahar Mollazadeh Beidokhti,

Jalil Vahdati-Khaki*

Department of Materials Science and Engineering, Engineering Faculty, Ferdowsi University of Mashhad, Mashhad, Iran

The authors confirm that the submitted manuscript has not been published previously and also is not under consideration for publication elsewhere. The authors also confirm that there are no known conflicts of interest associated with this publication.

Jalil Vahdati-Khaki